

Optimal Disturbance Structure and Development on a Sheared Interface

P. A. Yecko

Department of Physics and Astronomy
Arizona State University, Tempe, AZ 85287
and

Department of Astronomy
Columbia University, New York, NY 10027

Abstract

We present here flow fields –including three-dimensional velocity fields and interface deformations– associated with optimal disturbances in a two-phase shear flow. Optimal disturbances (OD) are a consequence of the transient growth dynamics fostered by the non-self-adjoint nature of the linear operator, in this case a generalization of coupled Orr-Sommerfeld and Squire operators. The base state consists of an initially flat interface with tension, across which the density, viscosity and mean velocity all change. In the immediate vicinity of the interface, boundary layer flow profiles match the tangential stress and velocity. In this work we focus on parameters characteristic of atomization in cryogenic rocket engine injectors, namely $Re = 1000$, $We = 150$ (based on liquid boundary layer thickness), density ratio $r = 0.02$ and viscosity ratio $m = 0.025$. The OD of this two-phase flow show some similarity to OD in ordinary boundary layers; among the important differences is the effect of transient growth on the shape of the interface. We show that strong up-flows and down-flows characterize the OD in the vicinity of the interface, that these up- and down-flows are present in both phases and appear to be coupled across the interface, leading to relatively large, streamwise-oriented interface deformations. Increasing the density difference or the viscosity difference leads to greater growth.

Introduction

When the onset of liquid breakup in the atomization regime can be observed in detail, three dimensional patterns are commonly seen on the deforming interface separating the two phases. Many such patterns involve remarkable finger-like structures, oriented approximately along the direction of flow, that emerge from the liquid. These streamwise-oriented ligaments (SOL) are often the immediate precursors of drop formation and, most importantly, their 3D nature defies an explanation in terms of a 2D stability analysis (although drop size predictions based on 2D theories have certainly been applied to cases where SOL are active). Complicating matters, SOL often co-exist with the more familiar 2D Kelvin-Helmholtz (KH) type instability, whose development can lead through wavecrest elongation to ordinary ligaments, oriented normal to the plane of the flow.

Streamwise patterns, not precisely SOL, are seen in high speed jets injected into quiescent air, as demonstrated by Hoyt and Taylor [1] and are also seen in planar jets as shown in [2], [3] and [4]. Sarpkaya and Merrill [5], however, see SOL in similar planar jets. On smaller scales, thin sheets such as those created by pressure swirl atomizers may also exhibit both streamwise-oriented patterns and SOL, even for experimental configurations ranging from flat to annular to conical sheet

geometries; see, e.g., [6] and [7].

Streamwise oriented ligaments in disintegrating liquids are most commonly seen when the ambient medium is co-flowing at high velocity. Good examples in the case of coaxial jets can be found in [8] and [9]. The airblasted planar layer studied by Raynal [10] clearly showed SOL in a simpler geometry. Lozano et al. [11] perform a rigorous investigation of SOL in airblasted sheets. Note that the thin sheet studies cited above also included airblast-type regimes and that these also exhibited streamwise oriented patterns.

Much of the work on coaxial jets concerns the formation of sprays in cryogenic rocket engines. In the regimes typical of this problem, the lengthscales of waves and patterns are small compared to the jet diameter, allowing the use of planar layers separated by an interface as a proxy for the coaxial jet geometry. Indeed, Hopfinger [12] and Yecko, Zaleski and Fullana [13] have pointed out that the relevant lengthscales are not those of the configuration, rather those which characterize the viscous boundary layers of the fluids. Related studies (e.g. Ref. [14]) have benefitted by using a plane mixing-layer configuration to study 3D structure formation. These works have also confirmed that 3D patterns are tightly linked to streamwise aligned vortices, at least for fluids of near equal density.

More recently, streamwise-oriented vortices and streamwise oriented structures have been intensely examined for their role in the transition to turbulence in a wide range of ordinary (one-phase) shear flows, including boundary layers, mixing layers and channel flows (i.e. Poiseuille, plane Couette). It is now clear that streamwise vortices in boundary layers are responsible for the high- and low-speed streaks ubiquitous at moderate Reynolds numbers. (A low speed streak is formed as the vortex lifts up slow fluid from the boundary layer into the free stream.) The streamwise vortices are not a modal instability, rather they are the consequence of the transient growth of special initial disturbances. Amplification factors for such disturbances can be large in any problem whose eigenfunctions are not orthogonal, even when all modes are damped. The disturbance which amplifies the most is called the *optimal disturbance* and can be thought of as a function which is not well “fit” by the eigenfunctions of the problem. The poor fit generally means that several coefficients will be very large in a superposition based on the eigenfunctions. In this way, as the eigenfunctions individually decay, the superposition can experience large transient growth.

In recent work [15]-[16] we have explored the possibility of strong 3D transient growth in a two-phase mixing layer configuration, concentrating on the growth factors and preferred wavenumbers. In that work, optimal disturbances were shown to be streamwise uniform, but to vary rapidly in the spanwise direction, consistent with the structure of many examples of SOL. Also in that work, parameter values such as Re and density ratio were not well suited to typical examples of primary breakup. Previously [13] we have also analyzed the 2D modal stability properties of this flow. The main purpose of the present study is to examine the actual optimal disturbances, in light of the possibility that by their nature (streamwise oriented) they may lead to a theory for the formation of streamwise-oriented ligaments. In this work we also present results of 3D modal stability calculations (NB: while it is possible to apply Squire’s transformation – Squire’s theorem, ensuring that 2D modes are most unstable, does not hold for this problem). Throughout this work, parameter are given values that are realistic for the injector atomization in cryogenic rocket engines.

There are relatively few 3D investigations of transient growth or optimal disturbances in a two-fluid shear flow with an interface. Notable exceptions are found in Refs. [3], [17]. Olsson and Henningson [18] examine 3D transient growth in watertable flow, where the less dense layer is neglected. In addition, some 2D studies have been done, such as [19] and [20]. These works stress that the computation of growth factors is non-convergent unless a proper energy norm is used (see also [21]) and concentrate on flows far removed from the atomization

regime.

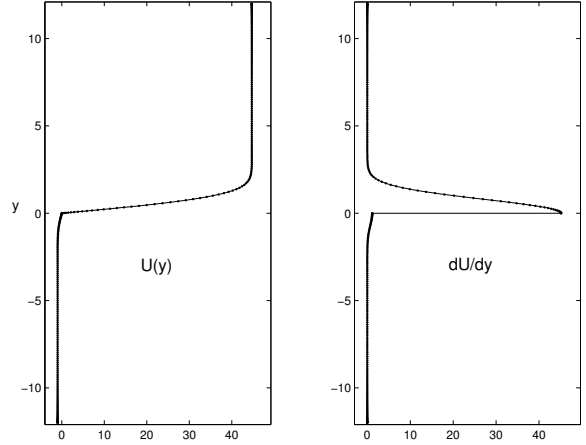


Figure 1. Base flow velocity (left) and velocity gradient (right).

Base Flow and Control Parameters

The starting point of this work is the incompressible Navier-Stokes Equations (subscript j is introduced to distinguish between the two fluids):

$$\nabla \cdot \mathbf{u}_j = 0 \quad (1)$$

and

$$\frac{\partial \mathbf{u}_j}{\partial t} + \mathbf{u}_j \cdot \nabla \mathbf{u}_j = -\frac{\nabla p_j}{\rho_j} + \frac{1}{Re_j} \nabla^2 \mathbf{u}_j + \frac{1}{We_j} \kappa \mathbf{n} \delta_I \quad (2)$$

where δ_I is a distribution on the interface, $\mathbf{u} = u\hat{x} + v\hat{y} + w\hat{z}$, and the notation is otherwise standard. Scaling has been performed using velocity scale U_j^* and length scale δ_j ; viscosity μ_j and density ρ_j are assumed constant within each fluid. The Reynolds number is based on the boundary layer thickness and is given as $Re_j = \rho_j U_j^* \delta_j / \mu_j$ while the Weber number is $We_j = \rho_j (U_j^*)^2 \delta_j / \sigma$.

Without loss of generality, we assume the lower layer consists of more dense fluid; quantities in this layer are thus identified by the subscript $i = L$, for liquid, while in the less dense upper layer fluid subscript $i = G$, denoting gas, is used. The basic state flow is $p_j = P = \text{constant}$ and $\mathbf{U} = U_j(y)\hat{x}$ where

$$U_j(y) = U_j^* \text{erf}(y/\delta_{L,G}) . \quad (3)$$

The above U profile is the solution of the *First Stokes Problem* and has characteristic thickness scale δ_j and constant velocity U_j^* far from the interface where $\delta_j = \sqrt{\mu_j t / \rho_j}$. In addition, the interface is assumed to be initially flat, $y = f(x, z, t = 0) = 0$. There is no restriction

that $U_G^* > U_L^*$ (as in airblast atomization) and fast liquid into slow ambient gas can also be described by this solution.

Velocity is continuous across the interface but its derivative experiences a discontinuity whose magnitude is proportional to the ratio of the viscosities, as demanded by the continuity of tangential stress: $\tau_L = \mu_L(dU_L/dy) = \tau_G = \mu_G(dU_G/dy)$ at the interface. Note that the velocity derivative is the negative of the base vorticity, $dU/dy = -\zeta = -\nabla \times U$. Continuity of velocity and the vorticity jump are clearly seen in Fig. 1.

This base flow is meant to capture essential elements of a two-fluid mixing layer and is somewhat idealized. For example, an $\text{erf}(y/\delta)$ profile is not a steady Navier-Stokes solution: the boundary layer thickness δ develops in time (or space). A stability analysis is thus performed on a snapshot of the profile at a particular time, under the assumption that any instability, to be relevant, must grow more quickly than the boundary layer develops. Assuming that the base flow evolved directly from an initial step function (or Kelvin-Helmholtz) profile, the boundary layers at time t must satisfy $\delta_G/\delta_L = \sqrt{(\mu_G/\rho_G)t}/\sqrt{(\mu_L/\rho_L)t} = \sqrt{m/r}$, while stress continuity requires $1/\sqrt{mr} = U_G^*/U_L^*$. Note the introduction of parameters describing the density ratio, $r = \rho_G/\rho_L$, and the viscosity ratio, $m = \mu_G/\mu_L$.

Disturbance Equations

The base flow (3) is perturbed by adding an infinitesimal disturbance (\mathbf{u}_j, p_j) . These linear perturbations can be assumed to have the form:

$$(\mathbf{u}_j, p_j) = (\hat{\mathbf{u}}_j(y, t), \hat{p}_j(y, t)) e^{i(\alpha x + \beta z)} \quad (4)$$

The resulting equations that govern the behavior of the perturbations can be written in terms of the normal velocity v_j and normal vorticity $\eta_j = i\beta u_j - i\alpha w_j$:

$$\begin{aligned} \frac{\partial}{\partial t}(D^2 - k^2)\hat{v}_j + i\alpha U_j(D^2 - k^2)\hat{v}_j \\ - i\alpha D^2 U_j \hat{v}_j - \frac{1}{Re_j}(D^2 - k^2)^2 \hat{v}_j = 0, \end{aligned} \quad (5)$$

$$\begin{aligned} \frac{\partial}{\partial t}\hat{\eta}_j + i\alpha U_j \hat{\eta}_j + i\beta D U_j \hat{v}_j \\ - \frac{1}{Re_j}(D^2 - k^2)\hat{\eta}_j = 0 \end{aligned} \quad (6)$$

where $k^2 = \alpha^2 + \beta^2$, $D = d/dy$, and boundary conditions: $\hat{v}_j = D\hat{v}_j = \hat{\eta}_j = 0$ hold far from the interface.

By assuming $\mathbf{q} = \tilde{\mathbf{q}}(\mathbf{y})e^{-i\omega t}$, an eigenvalue problem can be rewritten:

$$i\omega \mathbf{M}\tilde{\mathbf{q}}_j = \mathbf{L}\tilde{\mathbf{q}}_j \quad (7)$$

where $\mathbf{q}(\mathbf{y}, \mathbf{t}) = (v(y, t), \eta(y, t))^T$ and

$$\mathbf{M} = \begin{pmatrix} D^2 - k^2 & 0 & 0 & 0 \\ 0 & 1 & 0 & 0 \\ 0 & 0 & D^2 - k^2 & 0 \\ 0 & 0 & 0 & 1 \end{pmatrix},$$

$$\mathbf{L} = \begin{pmatrix} \mathcal{O}S_G & 0 & 0 & 0 \\ \mathcal{R}_G & \mathcal{S}Q_G & 0 & 0 \\ 0 & 0 & \mathcal{O}S_L & 0 \\ 0 & 0 & \mathcal{R}_L & \mathcal{S}Q_L \end{pmatrix}$$

and the matrix elements are:

$$\mathcal{O}S_j = i\alpha U_j(D^2 - k^2) - i\alpha D^2 U_j - \frac{1}{Re_j}(D^2 - k^2)^2,$$

$$\mathcal{S}Q_j = i\alpha U_j - \frac{1}{Re_j}(D^2 - k^2), \quad \text{and} \quad \mathcal{R}_j = i\beta D U_j$$

Using the above, we can define the matrix operator \mathcal{L} :

$$\mathbf{M}^{-1}\mathbf{L}\tilde{\mathbf{q}}_j = \mathcal{L}\tilde{\mathbf{q}}_j \quad (8)$$

Boundary and Matching Conditions

On the interface, a number of matching conditions must also hold, in particular, the normal velocity v is continuous:

$$v_G = v_L, \quad (9)$$

the streamwise velocity $u = ik^{-2}(\alpha Dv - \beta\eta)$ obeys:

$$\begin{aligned} (\omega - \alpha U) [\alpha(Dv_L - Dv_G) - \beta(\eta_L - \eta_G)] \\ = k^2(DU_G v_G - DU_L v_L), \end{aligned} \quad (10)$$

and the spanwise velocity $w = ik^{-2}(\beta Dv + \alpha\eta)$ continuity can be written:

$$\beta(Dv_L - Dv_G) = \alpha(\eta_G - \eta_L). \quad (11)$$

There are also conditions on the stress components; continuity relations of the tangential stresses τ_{xy}, τ_{zy} can be reduced to:

$$m(\beta D^2 v_G + \beta k^2 v_G + \alpha D\eta_G) = \beta D^2 v_L + \beta k^2 v_L + \alpha D\eta_L \quad (12)$$

and

$$mD\eta_G = D\eta_L. \quad (13)$$

The normal stress relation introduces the Weber number:

$$\begin{aligned} r(\omega Dv_G + \alpha DU_G v_G) - (\omega Dv_L + \alpha U_L v_L) \\ + \frac{m(D^3 v_G - 3k^2 Dv_G)}{iRe} - \frac{(D^3 v_L - 3k^2 Dv_L)}{iRe} \quad (14) \\ = -\frac{k^4}{iWe} f \end{aligned}$$

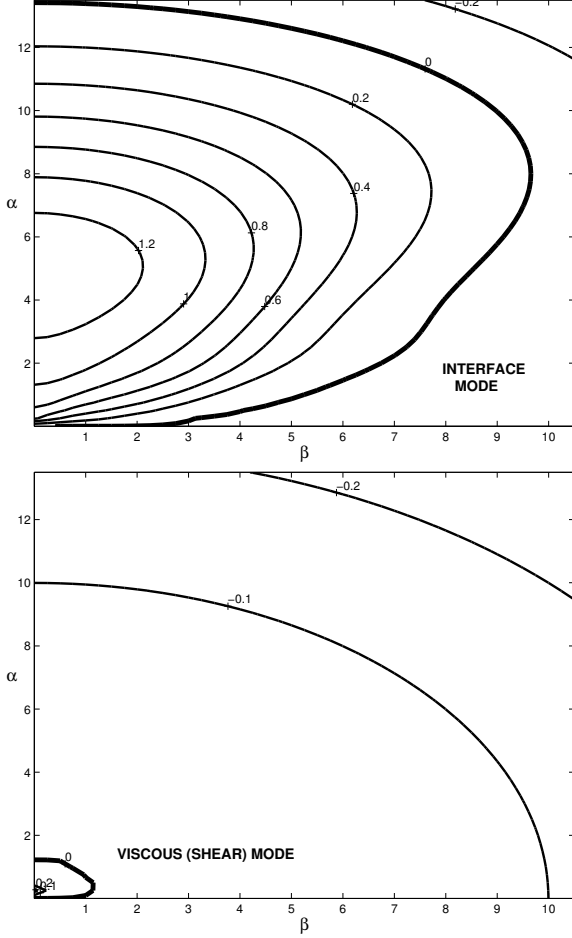


Figure 2. Growth rates (thin lines) and neutral curves (thick lines) for the interface mode (top) and first viscous, or shear, mode (bottom)

where the (scalar) free surface function f can be directly related to the interface velocity using the kinematic condition:

$$\frac{df}{dt} = (\partial_t + U\partial_x)f = v_G(0) = v_L(0) = v. \quad (15)$$

The disturbance problem in this form is used below to calculate: (i) the complete spectrum of eigenfunctions; and (ii) disturbances built from the eigenfunctions which experience the greatest transient amplification as a function of time and wavenumber. First we describe the numerical technique.

A Chebyshev collocation code developed in previous work [13] was used to evaluate the stability problem defined above. Transient amplification calculations were implemented according to the method given in [22]. To facilitate the expansion, the linear problem is mapped to the interval $[-1, 1]$ on which the Chebyshev polynomials

are orthogonal. The eigenfunctions can then be written as an expansion in a finite number N of Chebyshev terms $T_n(y)$ with unknown expansion coefficients, where N is the number of polynomials used, typically 150 or less per equation (600 total). Derivatives of eigenfunctions are evaluated using the recurrence relations based on linear combinations of lower order Chebyshev polynomials. Because of the infinite domain a continuous spectrum is present in addition to the finite discrete spectrum. In the calculations performed here, the infinite domain was approximated by a sufficiently large domain, a method known to be effective [23]. The eigenvalue problem is transformed into a corresponding $4N \times 4N$ matrix problem for the expansion coefficients including the boundary and matching conditions.

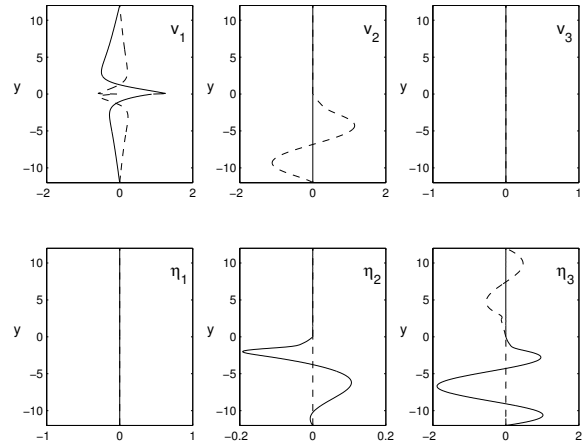


Figure 3. Normal velocity (v_n , top row) and normal vorticity (η_n , bottom) profiles in y for the two most unstable eigenfunctions ($n = 1, 2, 3$, left to right); $Re = 1000$, $We = 150$, $r = 0.02$, $m = 0.025$ and $(\alpha, \beta) = (1.0, 0.001)$; (v_1, η_1) is the interfacial (KH) mode.

Computing Transient Growth

Following the formulation of transient growth used in [25], let $G(t)$ represent the maximum possible energy amplification at time t , where G is optimized over all possible initial conditions for each instant in time. To measure the energy we require an appropriate norm; in this problem we use:

$$\begin{aligned} \|q\|_E = & \frac{1}{2k^2} \left[\int_{-L}^0 (|Dv_L|^2 + k^2|v_L|^2 + |\eta_L|^2) dy \right. \\ & + r \int_0^L (|Dv_G|^2 + k^2|v_G|^2 + |\eta_G|^2) dy \\ & \left. + \frac{k^4}{We} |f|^2 \right] \end{aligned}$$

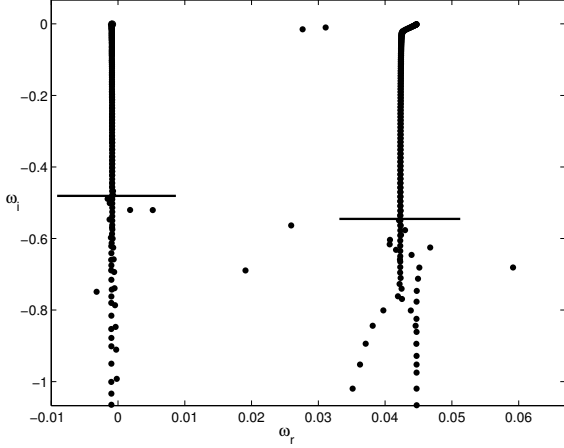


Figure 4. Spectrum of eigenvalues at $\alpha = 0.001$, $\beta = 1$, based on Chebyshev polynomial resolution $N = 120$; horizontal line segments denote ω_i values below which numerical error corrupts $G(t)$ calculations.

in which the interface makes a contribution proportional to surface tension ($\sigma \propto 1/We$). Renardy has pointed out [21] and South & Hooper have verified [19] that even in the absence of an interfacial energy (e.g. $\sigma = 0$, $r = 1$) the interfacial displacement must appear in the energy norm for the transient growth calculations to converge. This is discussed in more detail below.

We then define the growth factor:

$$G(t) = \sup_{\mathbf{q}(0) \neq 0} \frac{\|\mathbf{q}(t)\|_E^2}{\|\mathbf{q}(0)\|_E^2} = \|e^{i\mathcal{L}t}\|_E^2, \quad (16)$$

where \mathbf{q}_0 is an initial disturbance and \mathcal{L} is the linear operator defined above. This quantity $G(t)$ represents the maximum possible energy amplification at time t , optimized over all possible initial disturbances. The maximum or optimal growth is defined as $G_{max} = \sup_{t \geq 0} G(t)$, while a *peak* value $G_P \equiv \sup_{\alpha, \beta} G_{max}(\alpha, \beta)$ can also be computed. Note that G_{max} is associated with a particular initial disturbance which reaches G_{max} at a specific time t_{max} such that $G_{max} = G(t_{max})$. Similarly, there is a specific time t_p related to G_P .

The quantity $G(t)$ is obtained as follows. Assume that the eigenvalues of (7) are sorted in order of decreasing imaginary part ω_i . $G(t)$ can be approximated by computing the maximum possible energy amplification at time t , optimized over all possible initial combinations of the K eigenfunctions associated with the K least stable eigenvalues. In this case, it is possible to transform the energy norm of the matrix exponential (16) to an ordinary 2-norm via the following equation

$$\|e^{i\mathcal{L}t}\|_E^2 \approx \|\mathbf{F}e^{-i\Lambda t}\mathbf{F}^{-1}\|^2, \quad (17)$$

where Λ is a $K \times K$ diagonal matrix with the first K eigenvalues $\omega_1, \omega_2, \dots, \omega_K$ along the diagonal and \mathbf{F} is obtained by Cholesky factorization of $K \times K$ Hermitian matrix $\mathcal{M} = \mathbf{F}^H \mathbf{F}$ which is calculated using the inner product of the first K eigenfunctions, the inner product used being the same as the one defining the norm (\cdot) .

The approximation of (17) is a result of the finite number K used in the expansion. Following Reddy, Schmid and Henningson [24], K is chosen such that convergence is achieved. In practice, K must generally be large enough that near-degenerate eigenvalues of the spectrum are included in the approximation (this is discussed in more detail below in connection with modal results).

The 2-norm on the RHS of (17) can then be evaluated using SVD. This procedure gives both G_{max} and the K expansion coefficients of the disturbance associated with G_{max} [22, 23]. Note that, since eigenfunctions have been expressed as an expansion in Chebyshev polynomials, all calculations are ultimately performed in terms of the Chebyshev expansion coefficients. In particular, the energy norm (\cdot) and the weight matrix \mathcal{M} are easily recast in terms of the expansion coefficients using the properties of Chebyshev polynomials and their derivatives (for details see Ref. [24]).

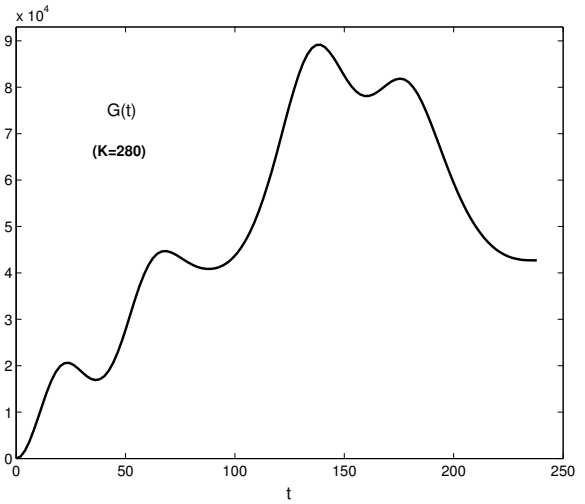


Figure 5. Transient growth factor $G(t)$ as a function of time t showing the occurrence of $G_{max} = 89200$ at $t = 138$; note $K = 280$ eigenfunctions were used here.

Modal Properties

Neutral Curves: We rapidly present in this section the three-dimensional neutral stability curves (see Fig. 2) for the flow parameters: $Re = 1000$, $We = 150$, $r = 0.02$ and $m = 0.025$, based on rocket engine conditions for

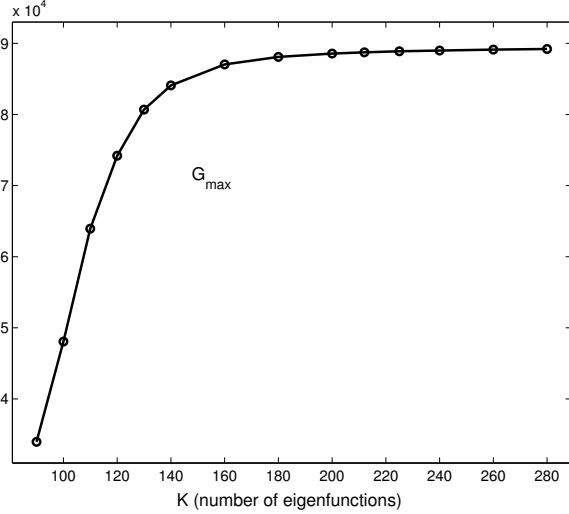


Figure 6. Maximum transient growth G_{max} as a function of the number of eigenfunctions K used to approximate the solution space; convergence is good for $K \approx 200$.

primary breakup of coaxial LOX-GH2. These values are taken from [12] and are based, like this study, on the use of liquid quantities for scaling. In particular, the liquid boundary layer thickness and velocity are taken as the characteristic length scale and velocity scale, respectively and used with the density and viscosity in forming the Reynolds and Weber numbers given above, from [12]. One can certainly make Squire’s transformation from the 3D stability problem to a 2D problem, but, in the case of two sheared fluids, Squire’s theorem is not necessarily valid. Note that the above parameter values also place the flow far from the marginal state that is the focus of Squire’s theorem. We must therefore anticipate that 3D modes might be more unstable than 2D modes. In Fig.2, however, we see that the largest growth rates of the two least stable modes are found for 2D modes; in the figures 2D modes are found along the vertical (α) axis.

The dominant feature of Fig. 2 is the large region of wavenumber space (i.e. the $\alpha - \beta$ plane) unstable to Kelvin-Helmholtz type instability thanks to the viscosity stratification of the base flow. In much of the literature, the KH mode is called the “interface mode,” a convention that we continue here. Note the small region of Tollmein Schlichting (TS) type instability simultaneously present, visible in the bottom panel of Fig. 2.

Transient growth, if it is to be important, should apparently be found outside these eigenvalue unstable regions and, in addition, should exhibit amplification factors that can compete with the most unstable modes in finite time. Below, we find exactly these transient growth

properties; but first, it is helpful to present a few more properties of the modal spectra.

Eigenfunctions: Like its better-studied Blasius boundary layer cousin, the single fluid erf() profile has both a discrete and a continuous spectrum made up of an infinite number of eigenvalues and eigenfunctions. Because our numerical technique is based on an expansion in a finite number N of Chebyshev polynomials, this spectrum is only found approximately. In practice we use $N = 600$, giving a sufficiently accurate and detailed spectrum. For completeness, we present here (see Fig. 3) the profiles of the two most unstable eigenfunctions at $\alpha = 1$, $\beta = 0$ for the flow parameters given above. For these wavenumbers the interface mode is unstable and the viscous mode is stable, as can be verified in Fig. 2. Mode 2 in Fig. 3, however, is not the viscous mode – rather it is a liquid Squire mode, as is apparent from the normal vorticity eigenfunction $\eta_2(y)$. Even though we have restricted the spectrum to 2D modes by choosing $\beta = 0$, we find that a Squire mode appears as the second most unstable mode after sorting the eigenvalues (NB: a pure Squire mode is always damped, however, even if weakly so). In an *ab initio* 2D formulation of the stability problem, a Squire equation is not solved and no Squire modes are found.

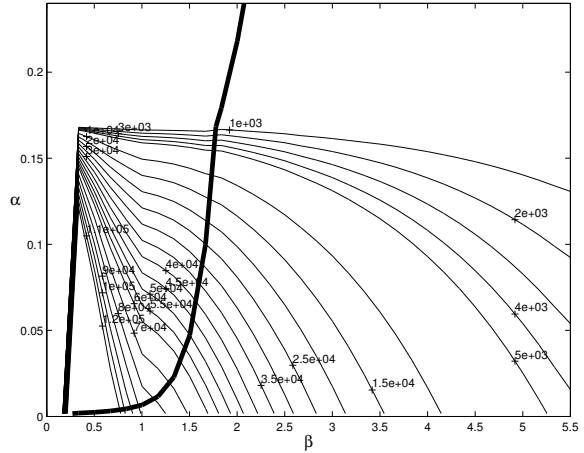


Figure 7. Level curves of G_{max} in the $\alpha - \beta$ wavenumber plane (thin lines) in the vicinity of the interface mode neutral curve (thick line, see also Fig. 2).

Spectrum: In principle, transient growth is a property of disturbances constructed from the entire modal spectrum. A numerical solution provides only a finite approximation of this spectrum, but in practice, an even smaller number of eigenfunction are needed to find a good approximation of transient growth. In Fig. 4 we present a portion of the computed spectrum at $\alpha = 0.001$, $\beta = 1$; at these wavenumbers all modes, even the interface mode, are stable and large transient growth factors

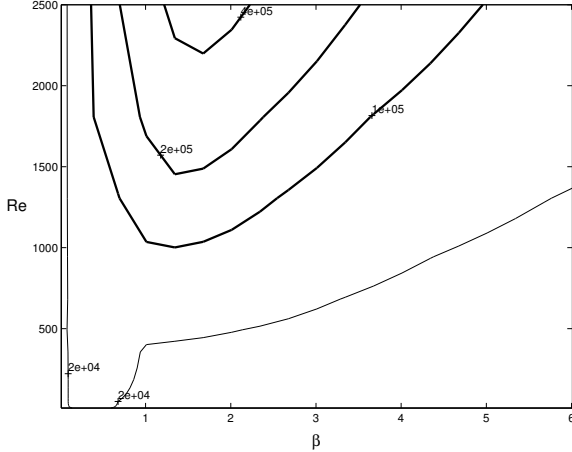


Figure 8. Level curves of G_{max} in the $\beta - Re$ plane for streamwise uniform disturbances ($\alpha = 0$).

(see below) are found. On the scale of Fig. 4 many familiar details of the eigenvalue spectrum of a shear flow are condensed beyond easy recognition at the top of the figure. What Fig. 4 clearly shows is the onset of numerical inaccuracy, which takes the form of scattered eigenvalues and branches from the vertical and can be seen only below the horizontal segments (these were added to the figure by hand). The number of eigenfunctions K used to compute transient growth should include as much of the spectrum as possible, but not include any modes from the numerically inaccurate region. We have generally used $K = 200$ or smaller and obtained good results. This is discussed in more detail in the next section.

Transient Growth

To get a complete picture of transient growth, it is necessary to compute the $G(t)$ and find its maximum G_{max} for every value (α, β) in the wavenumber plane. Before doing this, we examine the $G(t)$ function at a particular point, $\alpha = 0.001$, $\beta = 1$ (the same point at which the spectrum of Fig. 4 is found). In Fig. 5 we show $G(t)$ computed with $K = 280$ eigenfunctions, the largest number possible if numerically inaccurate values are shunned. Because it is computationally costly to calculate the time evolution of all possible combinations of these 280 functions, then find the best growth at every time t and then find the maximum over all t , we prefer to use $K < 280$.

In Fig. 6 we plot the maximum value G_{max} (for the conditions corresponding to Fig. 5) as a function of the number of eigenfunctions used to represent the disturbances. It is clear from the figure that (a) convergence is achieved as K is increased; and (b) accurate values of G_{max} are found already at $K \approx 180$. In the remaining

calculations, we adopt $K = 200$. We point out, too, that the growth factors are quite large, $G_{max} \sim O(10^5)$. Recall that in ordinary transient growth theory, G_{max} scales as Re^2 . It is not yet known whether this scaling is preserved in two-fluid shear flow with an interface.

Next, in Fig. 7, we show a very small region of the wavenumber plane where transient growth is strongest. Unlike in ordinary shear flows, transient growth of a sheared two-fluid interface must always compete with an unstable interface mode. In Fig. 7 we see that the region of largest G_{max} values directly adjoins the interface neutral curve (see also Fig. 2). Recall that for transient growth in ordinary shear, peak G_{max} values are usually found along the β axis (i.e. they have no streamwise variation); the same is true here.

Finally, since the peak growth occurs for $\alpha = 0$, we show in Fig. 8 the largest growth factors G_{max} in the $\beta - Re$ plane, for streamwise uniform ($\alpha = 0$) disturbances.

Optimal Disturbances

Finally, we present in Fig. 11 the full 3D flow fields and interface positions of the optimal disturbance for $Re = 1000$, $We = 150$, $r = 0.02$ and $m = 0.025$; here $\alpha = 0.001$ and $\beta = 1$. The panels of the top row show the vectors of normal and spanwise velocity (v, w) in the plane $x = 0$, looking downstream. The interface is centered at $y = 0$ in all the plots. The structure of the OD at $t = 0$ has several noteworthy features. First, highly focused up-flows are found in the (v, w) field in vicinity of the interface. These up-flows extend through the interface and are (partly) balanced by weaker, more diffuse down-flows, located halfway between each up-flow. In the u field at $t = 0$ (bottom left panel) we find relatively small velocities (and therefore energy). By the time of maximum growth ($t = t_P$), however, the u velocities have amplified tenfold, developing into strong streamwise jets, located just above the interface. At the same time the (v, w) field has changed dramatically (top right panel). While up-flows and down-flows are still present, the disturbance velocity in the $y - z$ plane is now concentrated in the liquid.

The interface displacement function f (middle row panels), which shows a doubly-periodic structure at $t = 0$, develops into a nearly streamwise-uniform pattern by $t = t_P$. Note that the G_{max} field in Fig. 7 does not show a clear maximum value outside the interface mode neutral curve. What we here call the optimal disturbance is thus somewhat different than the conventional definition. Still, it is clear from Fig. 7 that the largest growth is found for $\beta \sim O(1)$ and vanishing $\alpha \approx 0$. In the interest of generality we have chosen $\alpha = 0.001$ and $\beta = 1$ to depict the OD in Fig. 9. The non-zero value of α leads to interface deformations (Fig. 9 center row) that are slightly skewed away from exact streamwise orienta-

tion. At $\alpha = 0$ the OD would align precisely with the streamwise direction.

Density Ratio and Viscosity Ratio Effects

We have seen in the previous section that at $t = t_P$ the (kinetic) energy of the optimal disturbance appears to become concentrated in the strong streamwise jets (see Fig. 11, bottom left panel) located mainly in the upper, less dense layer. We can argue that for a larger density or viscosity ratio (corresponding to more closely matched values between the two layers) we expect to see weaker transient growth. This can be justified on the physical grounds that: (i) such a change in density or viscosity ratio implies a smaller fraction of the *base flow* energy is found in the upper layer; and so (ii) this weaker upper boundary layer flow will less effectively amplify the streamwise jets which closely correspond to the disturbance energy at maximum growth. This argument is confirmed by Fig. 9, although we admit that more rigorous calculations are required for proof.

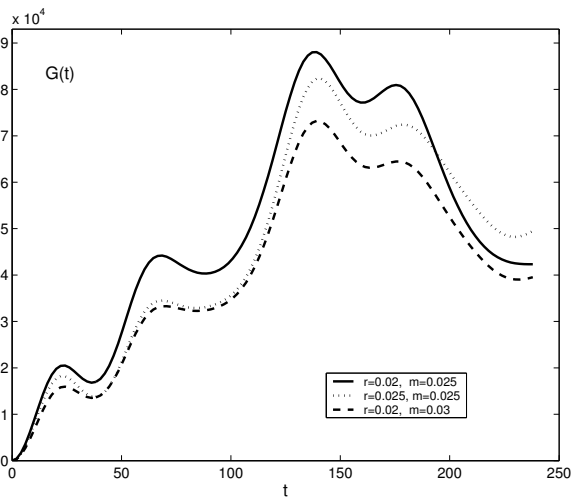


Figure 9. Dependence of the growth function $G(t)$ on a small change made to the density ratio (dotted) and to the viscosity ratio (dashed).

Conclusions

In this study we have presented a complete 3D calculation of the modal and transient growth properties of a two-fluid sheared interface flow typical of injection primary atomization in cryogenic rocket engines, leading ultimately to a detailed picture of the optimal disturbance and its development in time. Several of the characteristics of this OD are in good agreement with the characteristics of streamwise oriented ligaments often seen in coaxial and airblast primary breakup. We therefore ad-

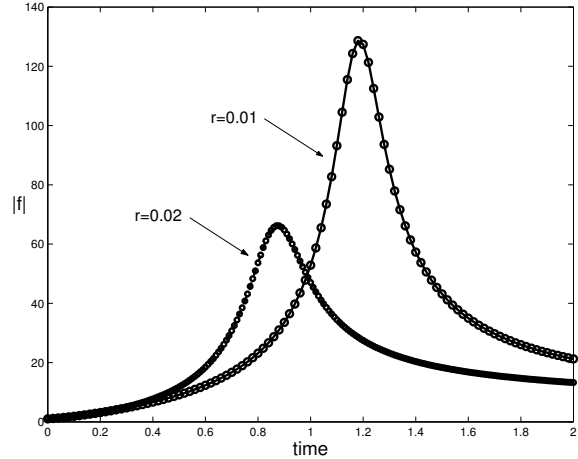


Figure 10. Interface displacement amplitude $f(t)$ such that $f(0) = 1$ for the optimal disturbance energy growth shown in Fig.5. Note that while peak energy growth occurs at $t = 138$, the interface displacement peaks much more quickly, before $t = 1$; for comparison, an identical calculation but with $r = 0.01$, a stronger density ratio, for which interface displacement peaks later but at greater value.

vance, on the basis of these results, a new model for the formation of streamwise-oriented ligaments, claiming that ligaments result from transient growth and are the nonlinear continuation of an optimal disturbance. We emphasize that predictive models for drop sizes in primary atomization are critically important in spray modeling applications. As yet, there is no fundamental theory for streamwise ligament formation even though this process is known to dominate drop formation in many cases. The model presented here cannot be conclusive until full 3D direct numerical simulations are performed which show transient growth and its role in the formation of streamwise oriented liquid ligaments.

References

- [1] J.W. Hoyt and J.J. Taylor. *Journal of Fluid Mechanics*, 83:119, 1977.
- [2] S.G. Durbin, T.P. Koehler, J.J.R. Reperant, M. Yoda, S.I. Abdel-Khalik and D.L. Sadowski. *Fusion Science and Technology*, 45(1):1–10, 2003.
- [3] L.D. Söderberg *Journal of Fluid Mechanics*, 493:89–119, 2003.
- [4] A. Konkachbaev, N.B. Morley and M.A. Abdou. *Fusion Engineering and Design*, 63-64:619–625, 2002.

- [5] T. Sarpkaya and C.F. Merrill. *AIAA Journal*, 39(7):1217-29, 2001.
- [6] B.E. Stapper, W.A. Sowa and G.S. Samuelson. *Journal of Engineering for Gas Turbines and Power*, 114:39-45, 1992.
- [7] A. Mansour and N. Chigier. *Physics of Fluids A*, 2(5):706-19, 1990.
- [8] P. Marmottant and E. Villermaux. in *Combustion dans les moteurs fusees, CNES Colloque*, Cépaduès, Toulouse, 2001.
- [9] J.C. Lasheras and E.J. Hopfinger. *Annual Review of Fluid Mechanics*, 32:275-308, 2000.
- [10] L. Raynal. *Instabilité et entraînement a l'interface d'une couche de mélange liquide-gaz* PhD Thesis (Université Joseph Fourier, Grenoble, 1997).
- [11] A. Lozano, F. Barreras, G. Hauke and C. Dopazo. *Journal of Fluid Mechanics*, 437:143-73 (2001).
- [12] E.J. Hopfinger. in *Combustion dans les moteurs fusees, CNES Colloque*, Cépaduès, Toulouse, 2001.
- [13] P. Yecko, S. Zaleski and J.-M. Fullana. *Physics of Fluids*, 14(12):4115-23, 2002.
- [14] J.C. Lasheras and H. Choi. *Journal of Fluid Mechanics*, 189:53-86, 1988.
- [15] P.A. Yecko. *Proc. International Congress of Liquid Atomization & Spray Systems (ICLASS)*, Sorrento, Italy (2003).
- [16] P.A. Yecko. *Proc. Institute of Liquid Atomization & Spray Systems (ILASS) Americas*, Monterey, CA (2003).
- [17] L. de Luca, M. Costa and C. Caramiello. *Physics of Fluids*, 14(1):289-99, 2002.
- [18] P.J. Olsson and D.S. Henningson. *Studies in Applied Mathematics*, 94:183-210, 1995.
- [19] M.J. South and A.P. Hooper. *Journal of Fluid Mechanics*, 381:12-, 1999.
- [20] T.L. van Noorden, P.A.M. Boomkamp, M.C. Knaap and T.M.M. Verheggen. *Physics of Fluids*, 10(8):2099-3001, 1998.
- [21] Y. Renardy. *Physics of Fluids*, 30(6):1627-37, 1987.
- [22] S.C. Reddy and D.S. Henningson. *Journal of Fluid Mechanics*, 252:209-, 1993.
- [23] K.M. Butler and B.F. Farrell. *Physics of Fluids A* 4(8):1637, 1992.
- [24] S.C. Reddy, P.J. Schmid and D.S. Henningson. *SIAM Journal of Applied Mathematics*, 53(1):15, 1993.
- [25] P.J. Schmid and D.S. Henningson. *Stability and Transition in Shear Flows*. Springer Verlag, New York, 2000.

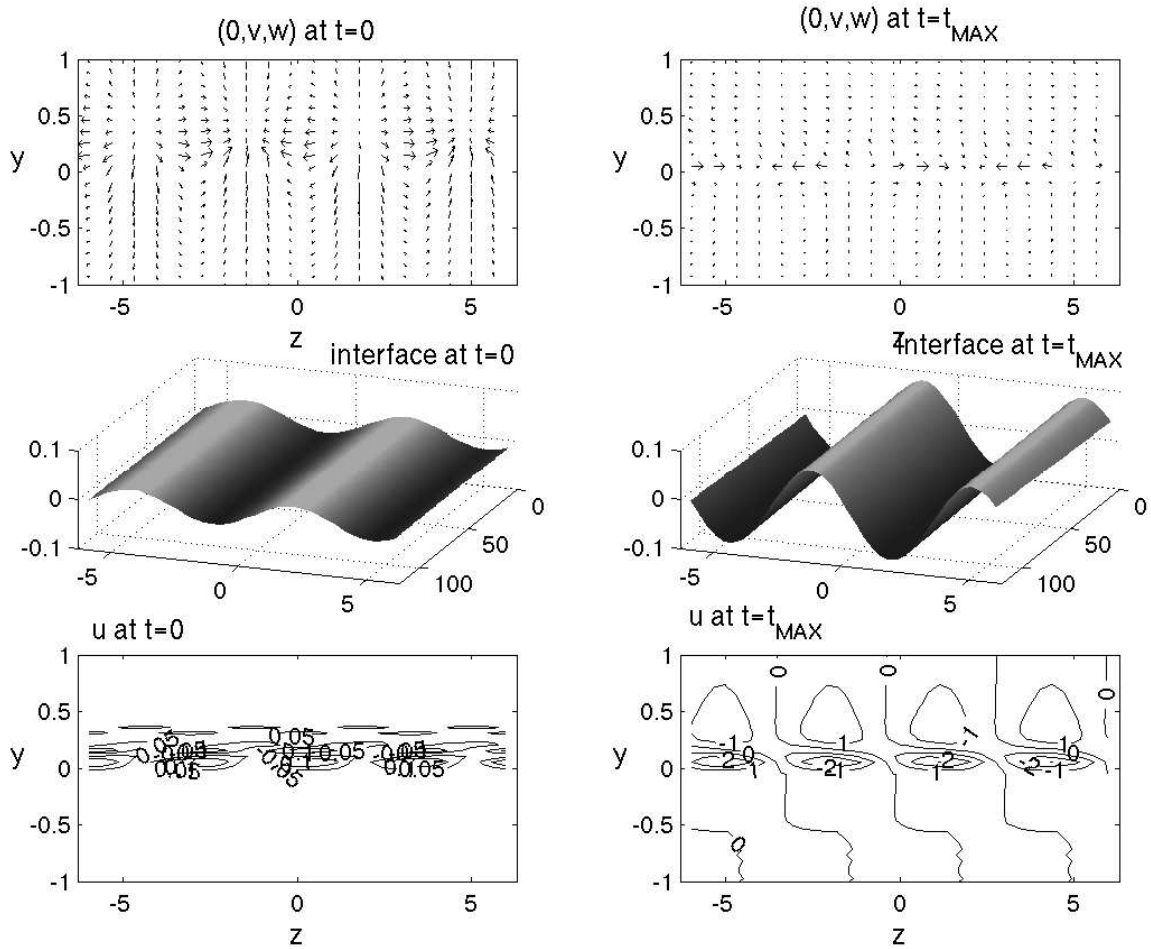


Figure 11. Optimal disturbance flow fields at $t = 0$ (left column) and at $t = t_{max}$ (right column); shown are the vectors $(0, v, w)$ looking downstream (top row), the interface (center row, magnified ten times), and the downstream velocity u (bottom row).